Liquid Crystals
Publication details, including instructions for authors and subscription information:
http://www.informaworld.com/smpp/title~content=t713926090

Cholesteric liquid crystals: Image contrast in the TEM

Timothy J. Bunning[a]; Deborah L. Vezie[b]; Pamela F. Lloyd[c]; Peter D. Haaland[d]; Edwin L. Thomas[b]; W. Wade Adams[a]
[a] Wright Laboratory, Materials Directorate, Ohio, U.S.A. [b] Dept. of Materials Science and Engineering, MIT, Cambridge, Massachusetts, U.S.A. [c] UES Inc., Dayton, Ohio, U.S.A. [d] Lawrence Associates Incorporated, Dayton, Ohio, U.S.A.

To cite this Article Bunning, Timothy J. , Vezie, Deborah L. , Lloyd, Pamela F. , Haaland, Peter D. , Thomas, Edwin L. and Adams, W. Wade(1994) 'Cholesteric liquid crystals: Image contrast in the TEM', Liquid Crystals, 16: 5, 769 — 781
To link to this Article: DOI: 10.1080/02678299408027849
URL: http://dx.doi.org/10.1080/02678299408027849

LIQUID CRYSTALS, 1994, VOL. 16, NO. 5, 769–781

Cholesteric liquid crystals: image contrast in the TEM

by TIMOTHY J. BUNNING*†, DEBORAH L. VEZIE‡, PAMELA F. LLOYD§, PETER D. HAALAND¶, EDWIN L. THOMAS‡ and W. WADE ADAMS†

† Wright Laboratory, Materials Directorate, WL/MLPJ, Bldg 651, 3005 P. St., Ste.1, Wright-Patterson Air Force Base, Ohio 45433, U.S.A.
‡ Dept. of Materials Science and Engineering, MIT, Cambridge, Massachusetts 02139, U.S.A.
§ UES Inc., 4401 Dayton-Xenia Rd., Dayton Ohio 45432, U.S.A.
¶ Lawrence Associates Incorporated, 5100 Springfield Pike, Suite 509, Dayton, Ohio 45431, U.S.A.

(*Received 8 July 1993; accepted 30 September 1993*)

Bright-field image contrast of thermotropic cholesteric liquid crystalline materials in the transmission electron microscope (TEM) is investigated. Possible sources of contrast for these systems are discussed in terms of their molecular anisotropy. A cholesteric side-chain liquid crystalline compound was investigated with TEM, low voltage high resolution scanning electron microscopy (LVHRSEM), and atomic force microscopy (AFM) to determine the origin of the strong contrast observed in these systems using bright-field transmission electron microscopy. Initial contrast of thin microtomed sections, as viewed with TEM low dose techniques and an image intensifier, was much weaker than observed under normal viewing conditions. The periodic steady state contrast typically observed for these materials is the result of beam damage. Furthermore, the surface of microtomed samples (parallel to the cholesteric helical axis) is corrugated with a periodicity of 1/2 the pitch due to a preferred fracture path in the glassy cholesteric state. AFM profile analysis shows an average peak to valley height of approximately 20–25 nm. AFM of free surfaces from aligned films also indicates a corrugation with a periodicity equal to 1/2 the pitch with substantially smaller average corrugation depths. TEM indicates a series of $+1/2$ and $-1/2$ disclination lines at the surface due to a rotation of the preferred helix direction parallel to the surface, consistent with previously reported models.

1. Introduction

Electron microscopy techniques have been utilized to examine defect structures in liquid crystalline materials, specifically lyotropic cholesteric phases derived from biological systems [1–3]. Recently electron microscopy techniques have been extended to include the investigation of thermotropic liquid crystalline materials including images of individual smectic and crystalline phases using transmission electron microscopy (TEM) [4–7]. Lamellar decoration combined with amine etching have been used to investigate directly the surface topography of defect structures in nematic polyesters with TEM and LVHRSEM [8–10]. Several low molecular weight liquid crystalline systems have also recently been imaged while adsorbed onto graphite using scanning tunnelling microscopy [11, 12].

* Author for correspondence.

0267–8292/94 $10·00

SEM of cholesteric liquid crystalline compounds in a glassy phase yields information about the periodic nature of the helical structure. Fracture parallel or oblique to the helical axis produces a periodic surface topography due to the spatially varying molecular directors (**n**) which can be imaged on fractured bulk films [13–15]. When the fracture surface is exactly parallel to the helical axis, the surface periodicity corresponds to one-half the pitch (P) as there is no difference between the $+\mathbf{n}$ and $-\mathbf{n}$ directors. A model based on preferential crack propagation in spatially varying anisotropic glasses predicts the contour of the fracture surface relative to the helical direction [16]. Various types of defects can also be observed in these fracture surfaces.

Information about the pitch (P) can also be obtained from TEM, as microtomed sections exhibit a series of alternating dark and bright bands whose distance corresponds to one-half the pitch of the cholesteric helix. Although several authors have reported this banded contrast variation [17–20], no adequate explanation of the contrast mechanism has yet been proposed. We discuss here possible sources of this contrast and investigate these using LVHRSEM, TEM and AFM.

2. Experimental procedure

The cholesteric materials investigated (see figure 1) are a class of cyclic siloxane materials [21]. The compound examined for this work had a P/Q ratio of 1 where P corresponds to the number of biphenyl-4-allyloxybenzoate side chains and Q corresponds to the number of cholesteryl-4-allyloxybenzoate side chains. This material has a T_g at 50°C, a wide cholesteric mesophase, and a clearing temperature of 220°C. Films, formed by heating the compound to 150°C followed by shearing, exhibit a Grandjean texture where the helical axes are perpendicular to the film surfaces. These films exhibit selective reflection at 514 nm (refractive index = 1·5) at room temperature

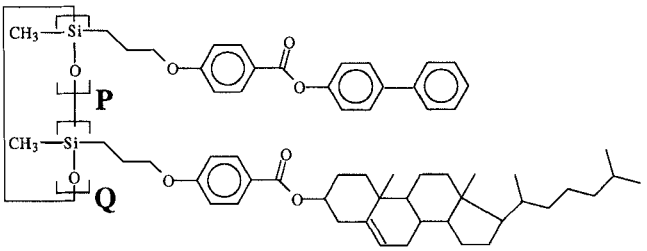

P + Q = 5 : P/Q = 1

(*a*)

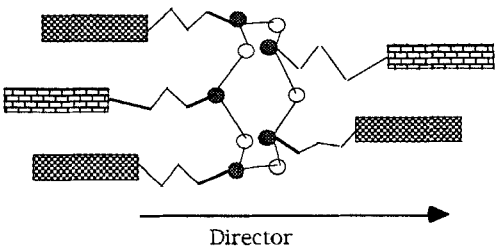

(*b*)

Figure 1. (*a*) Chemical structure of cyclic siloxane-based side-chain cholesteric liquid crystalline materials. The composition of the material investigated had equal amounts of the two mesogens attached. (*b*) Possible conformation of mesogenic groups relative to the siloxane ring.

as measured with an integrating sphere. Quenching from the mesophase to room temperature allows the glassy mesophase to be obtained.

Bulk films, sheared between Teflon sheeting which was subsequently removed, were embedded in a room temperature epoxy system and sections were taken parallel to the helical axis. Imaging is approximately perpendicular to the helical axis. LVHRSEM was performed using a Hitachi S-900 FEG SEM operated at 0·8–1·0 keV accelerating voltage. LVHRSEM samples were coated with approximately 10 Å of tungsten using a VCR dual ion beam coater. TEM was performed on a JEOL 100CX at 100 keV and images were recorded on Kodak SO163 film. Microtomed sections were 60–80 nm thick. Free surfaces of a Grandjean aligned sample on silicon wafers (rather than Teflon sheeting) were also investigated. Film preparation was the same except that the top and bottom silicon wafers were slid apart. Low dose TEM was performed on a JEOL 200CX using a Gatan image intensifier and VCR to capture dynamic data. TEM negatives were scanned using a Molecular Dynamics densitometer and analysed using ImageQuant Software. AFM was performed with a Park Scientific SFM-BC2-210 Scanning Force Microprobe running from a SPC-400 Scanning Microprobe Central Control Unit. A standard silicon nitride tip with a radius of curvature of approximately 40 nm was used with mid-range forces in the repulsive mode. AFM was performed on the microtomed samples on TEM grids fixed to the AFM mount.

We restrict our analysis of the TEM, LVHRSEM, and AFM data to those images in which the structural repeat corresponded to approximately 1/2 the pitch (thus our viewing direction is normal to the helical axis).

3. Results and discussion

The bright-field image contrast in a transmission electron microscope will depend on the variation of scattering power across the sample. Both amplitude and phase contrast differences can contribute to overall image contrast.

Amplitude contrast can arise from two subcategories—mass thickness differences and/or variations in the scattered intensity due to material anisotropy (for example, Bragg scattering for crystals). Several physical traits contribute to mass thickness contrast including compositional variations in multicomponent systems, density variations in single component materials, and thickness variations throughout the sample. All of these may change with electron exposure due to beam-induced changes in sample composition. Chain scission and cross-linking can lead to preferential changes in thickness or projected density.

Phase contrast arises from variations in the projected inner potential which is proportional to the mass thickness for a sample with a homogeneous composition. For an anisotropic system, the projected density can be somewhat larger for certain projections (for example, down-axis orientation) of the molecules as there will be a higher number of atoms in the column, since intramolecular distances are shorter than intermolecular ones. If the sample thickness is constant, then the only variations in projected inner potential will be from projected density variations. By under-focusing the objective lens, regions of higher projected density will appear darker. Optimum phase contrast (for the object periodicity $P/2$ of approximately 170 nm considered here) requires a very large defocus (about 10^3 microns) and would result in a loss of image resolution. Significant phase contrast is obtainable by using a defocus, ΔZ, of a few microns without sacrificing resolution.

Several groups [17, 18, 20, 22] have observed alternating dark and light bands in bright-field TEM in thin microtomed sections of various cholesteric materials without

addressing the source of this contrast. If one *assumes* sections are of constant thickness, then the source of contrast in a bright-field *in-focus* image must arise from the material anisotropy, i.e. from the helical arrangement of the molecules. The dark and bright regions of an in-focus image would correspond to locations where the electron beam is alternatively parallel to and perpendicular to the molecular axis (helical axis assumed to lie in plane of the section and hence normal to the beam direction) as shown in figure 2. The contrast would then result from relative scattering differences from regions I and II due to different amounts of intensity scattered at angles beyond that subtended by a particular objective aperture. The distribution of scattered intensity from a nematic region normally consists of a strong equatorial ring due to intermolecular interference and weaker scattering on meridional planes due to the periodic variation of structure along the molecular axis. If a small objective aperture is used such that the equatorial intermolecular scattering maximum is outside the aperture, the image intensity will be diminished in proportion to the extent of the equatorial scattering ring which is excited. Region I will have fewer scattered electrons blocked from the BF image than region II, since the Ewald sphere will intersect the equatorial ring in only two locations, whereas with the electron beam incident along the molecular axis, the full ring can be excited. Therefore, regions where the molecular axis is parallel to the electron beam will appear darker than the regions with in-plane orientation of the molecular axis relative to the film. A reversal of the dark and bright regions could occur if the molecular scattering is stronger along the meridian. In any case, the actual variation of intensity along the in-plane helical axis will depend on the relative amount of scattered intensity intersected by the Ewald sphere at angles greater than that of the objective aperture as a function of beam–sample orientation. A consequence of this model is that by tilting the specimen about an axis parallel to the helical twist axis, the bright and dark regions will simply translate along the axis of tilt as given by equation (1),

$$d = \frac{P\Theta}{2\pi}, \tag{1}$$

where d is the distance translated, P is the pitch of the cholesteric, and Θ is the angle of tilt.

Another feature of this orientation dependent scattering contrast is the effect of electron beam radiation damage. Since the inelastic interaction of the high energy electron beam with the organic material will cause crosslinking and chain scission normally resulting in substantial loss of molecular order, the BF image contrast which depends on the variation in molecular orientation will diminish or disappear at high electron dose as the beam damaged sample loses orientational order. This aspect of the contrast can be readily assessed by viewing the electron diffraction pattern and bright field image as a function of dose.

If mass thickness contrast is present due to thickness variations arising from the microtoming process, the thicker regions will correspond to enhanced scattering contrast and will appear dark. However, upon tilting the specimen about the helical axis, contrast arising from thickness variations should be invariant, thus easily distinguishing this mechanism of image contrast from diffraction contrast as discussed above.

Since most organic compounds are beam sensitive [23, 24], low dose conditions (10^{-3} C cm^{-2} s^{-1}) were first employed to establish that amplitude contrast was present. At very low dose, contrast was found to be very weak and the overall contrast

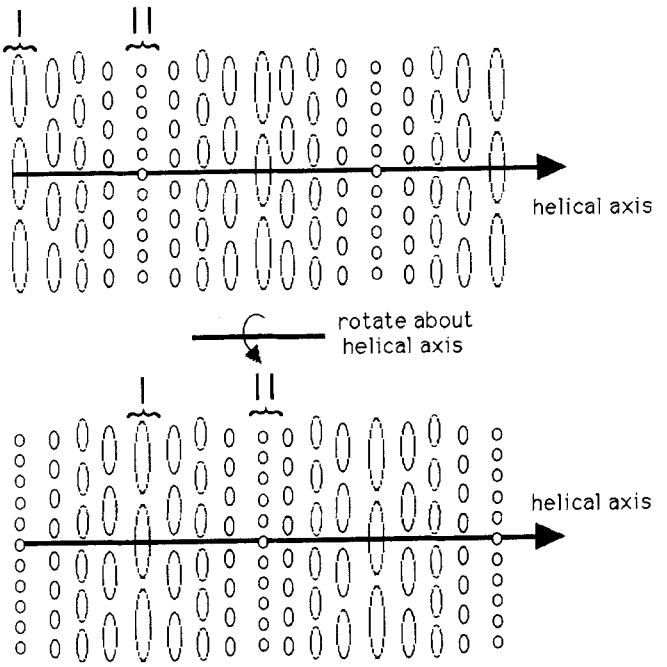

Figure 2. Schematic of molecular orientation perpendicular to the helix and the change in direction of these directors as the sample is rotated around the helical axis.

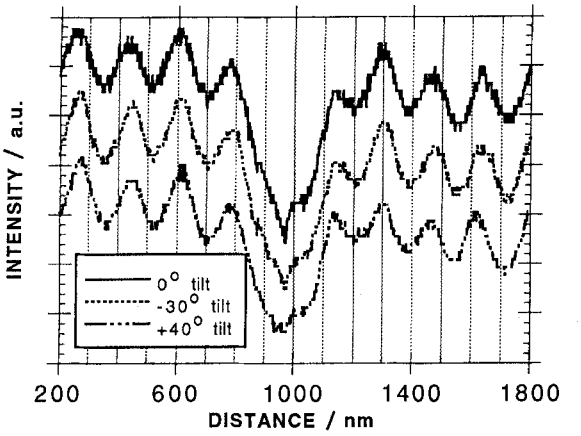

Figure 3. Microdensitometer curves from a series of tilt experiments showing no translation of the contrast bands.

was enhanced quickly with increasing dose. Thus, at normal operating conditions where the beam dose rate is in the range of 10^1–10^3 C cm^{-2} s^{-1}, a large increase in the contrast has developed due to beam damage of the material before the viewer can notice. Coupled with the development of this contrast was the rapid disappearance (0·5 s-equivalent to a dose of 5×10^0–10^2 C cm^{-2}) of an initially oriented electron diffraction pattern observed when using a small (7 μm diameter) selected area diffraction aperture. It is unclear what percentage of the *initial* contrast is attributable to diffraction contrast as it is too short-lived to perform a tilt-series. However, the

(*a*)

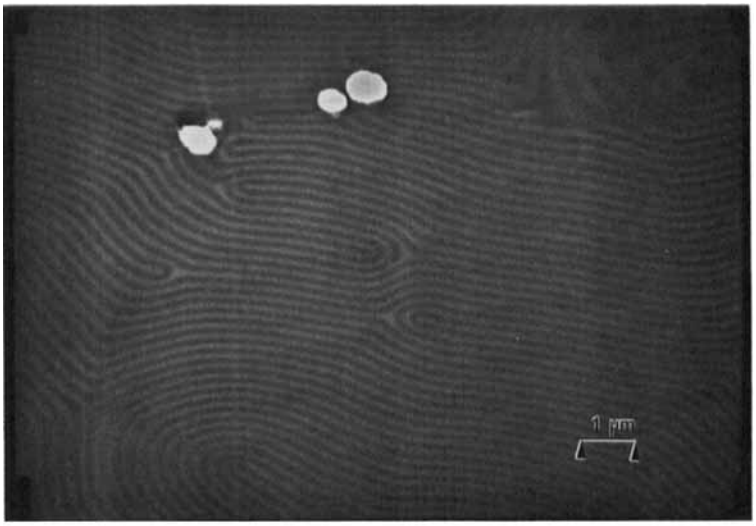

(*b*)

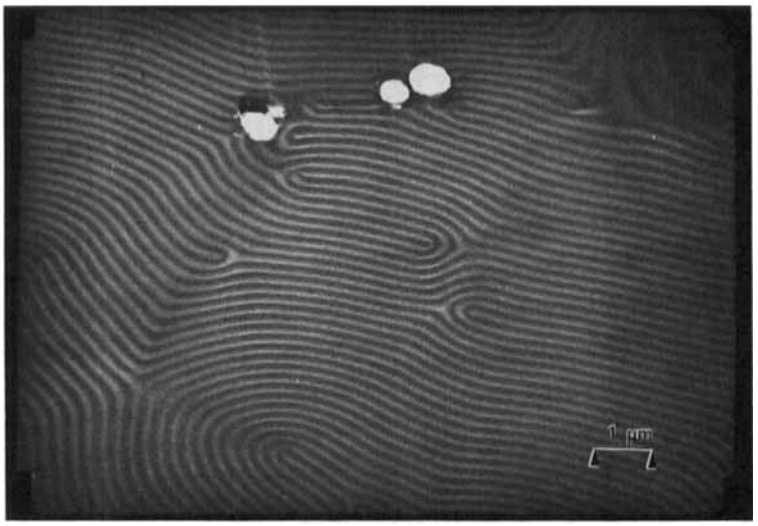

(*c*)

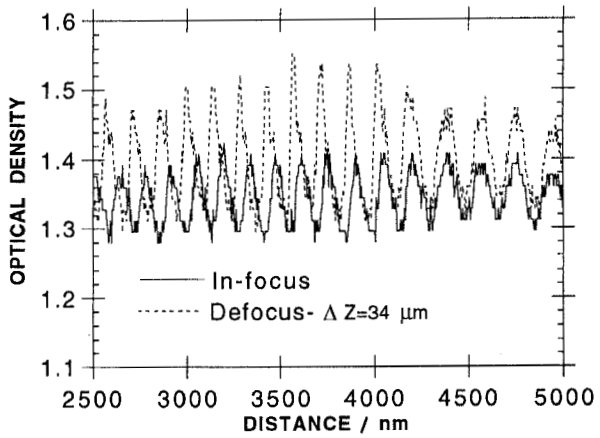

Figure 4. (*a*) In-focus TEM micrograph taken under normal dose conditions. (*b*) Same region as in (*a*) but defocused $\approx 34\,\mu m$. Stronger contrast is observed. Note the Fresnel fringes around the holes. (*c*) Microdensitometer traces of negatives from (*a*) and (*b*).

increase in contrast with the absence of any significant orientation in the diffraction pattern indicates that diffraction contrast is *not* a contributing mechanism for the steady-state samples.

Further proof that diffraction contrast is not present can be obtained from the tilt experiment discussed previously. Microtomed sections were imaged under normal dosage conditions in the TEM while being tilted about the helical axis, which is perpendicular to the alternating bright and dark bands. A full 90° rotation was approached by tilting a section $+40°$ and $-30°$. The microdensitometry scans in figure 3 clearly show that no shift in contrast was observed with tilt. The large intensity dip in the centre of the scan was caused by a piece of dirt and was used as a reference point. Neither the pitch periodicity nor the contrast modulation changed with tilt. The periodicity corresponded to $P/2$ and averaged about 170 nm.

An in-focus BF image of a section of the vitrified cholesteric liquid crystal is shown in figure 4 (*a*) under normal viewing conditions (beam damage has occurred). Since the micrograph was recorded approximately in-focus, the contrast present is due only to the variation of scattering power outside the objective aperture. The periodicity of the alternating bright and dark lines of 165 nm matches closely the $P/2$ value of 170 nm based on selective reflection measurements. When defocused by $\Delta Z \approx -34\,\mu m$, as shown in figure 4 (*b*), the contrast is substantially enhanced as shown in the densitometer trace, figure 4 (*c*).

LVHRSEM and AFM were used to examine the surface of both unirradiated and TEM irradiated microtomed samples. Figure 5 (*a*), an AFM image of an unirradiated sample, reveals a highly corrugated surface with a periodicity (167 nm) close to one-half the pitch of the sample. Beam damage effects such as mass loss and/or dimensional changes can be excluded as a cause of the corrugated topography for these samples as they had not been irradiated with the electron beam. An edge dislocation with a Burger's vector of **P** is shown in the middle of the scanned area in figure 5 (*b*). The 3-dimensional structure of the surface is shown in figure 5 (*c*) and height profile analysis indicates an average peak to valley height of 20–25 nm.

Interestingly, the free surfaces of cast films also reveal topography when examined with AFM. For a planar (Grandjean) sample, the helix direction in the bulk of the film is normally perpendicular to the surface plane. Near the surface, the twisted structure of the bulk material cannot readily adapt to the surface boundary condition. One solution to this boundary problem is a series of alternating $+1/2$ and $-1/2$ disclination lines at the surface which was observed with bright field TEM as shown in figure 6 (*a*). This has been previously observed optically for large pitch materials and attributed to a low energy packing conformation of the helices [25] as shown in figure 6 (*b*). In this orientation, the helical axis lies parallel to the surface plane instead of perpendicular as in the bulk. The interface between these two orientations gives rise to the series of $+1/2$ and $-1/2$ disclinations as shown. Note that the surface topography shown by Saupe [25] is flat (see figure 6 (*b*)), while the surfaces observed with TEM possess undulations whose periodicity corresponds to one-half the pitch. Free surfaces of these cast films were observed with AFM to verify the surface topography. A complex surface topography was observed as shown in figure 6 (*c*). The periodicity again corresponded to $P/2$, but the depth profile analysis indicated much shallower corrugation, of the order of 2–4 nm. No surface topography was evident when examined with LVHRSEM.

The surface of a microtomed stub was also examined, Since this constitutes the surface region of a very thick film, mechanical stresses giving rise to buckling phenomena should be minimized. If buckling stresses caused the thin microtomed

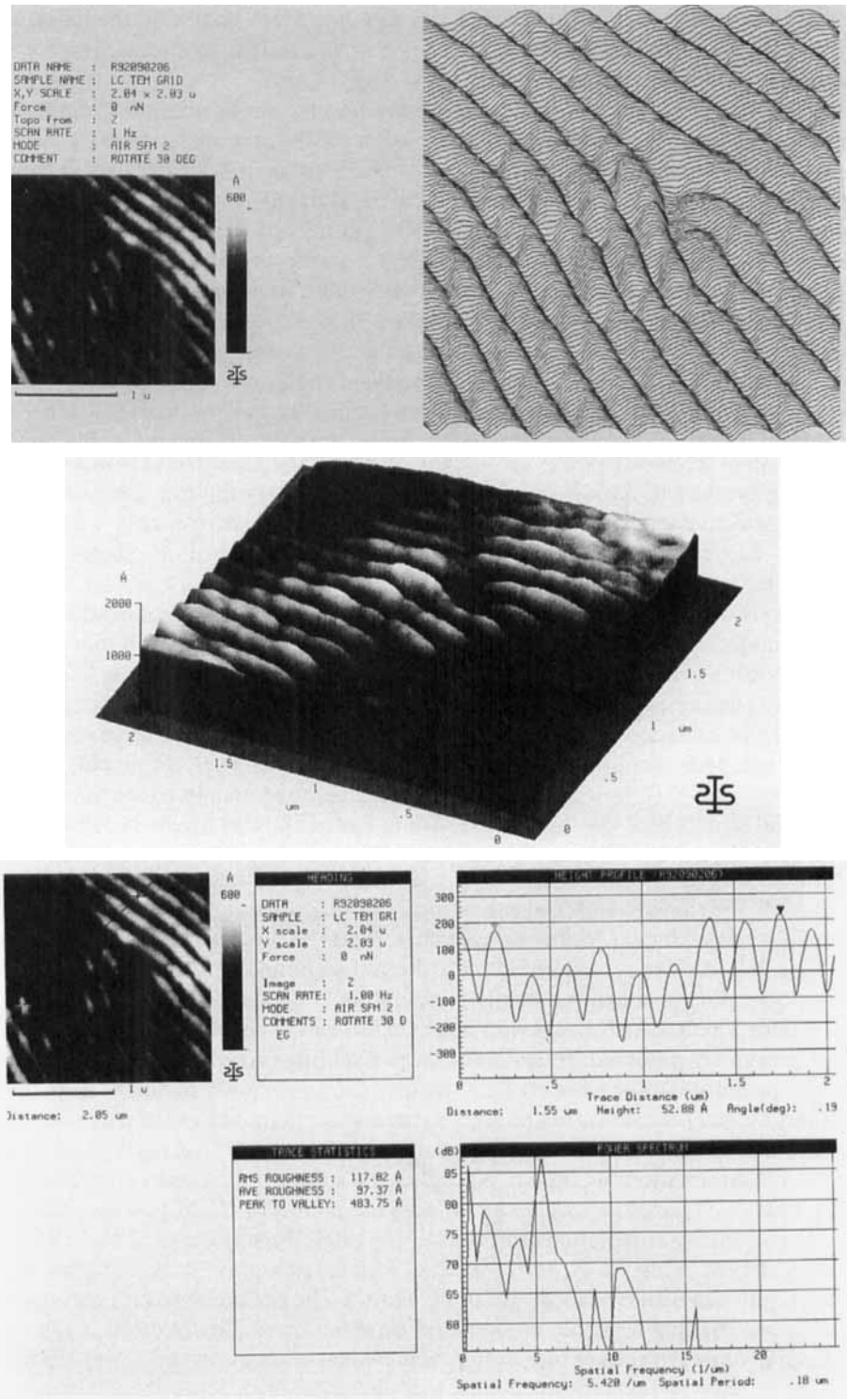

Figure 5. (*a*) AFM image of the surface of an unirradiated microtomed sample. (*b*) The same area in three dimensions. (*c*) Height profile analysis across this section.

sections to warp and produce contrast, then one would expect the stub to be nearly flat due to its 'infinite' thickness. The surface of this bulk sample exhibited the *same* corrugated surface texture with similar height modulation in AFM as the microtomed thin sections.

The periodic surface topography in microtomed sections is thought to be due to preferential crack propagation as the sections are microtomed, rather than relaxation of the thin section after cutting. Indeed, the surface structure of sections microtomed parallel to the helical axis looks the same as bulk fracture surfaces observed in the LVHRSEM as shown in figure 7. AFM of these bulk fracture surfaces reveals topography similar in nature to that shown in figure 5 with comparable peak to valley heights. The fracture path tends to minimize the surface area exposed, but locally the crack tip is preferentially propagated relative to the orientation of the molecules, thus producing a sinusoidal fracture surface. When the microtome direction is parallel to the plane of the helical axes, two fracture paths are favoured as shown in figure 8 [26]. Assuming constant density, the first fracture path results in the maximum mass thickness difference (case I), while the second results in no mass thickness difference (case II). Based on the above reasoning, *undamaged* microtomed sections fractured parallel to the helical axis and viewed normal to this axis should show no contrast based on mass thickness approximately 50 per cent of the time. While we did not conduct extensive studies of the sections under low dose conditions, frequently only a slight contrast was observed suggesting that the fracture paths at the top and bottom surfaces possessed only a small phase difference (nearly case II).

Since both the beam direction and the plane of the section are perpendicular to the helical axis and the long range order extends in the plane to many tens of microns (see figure 4(*a*)), it is reasonable to assume correlation of the molecular directors through the thickness of a section. Thus one *cannot* deduce that one orientation of molecules lies in the dark bands, while the other orientation lies in the white bands as has been previously stated in the literature [17]. A peak on one side of the microtomed section corresponds to a valley on the complementary stub surface, although both regions possess the same director orientation.

The large increase in the contrast with beam damage leads to interesting speculation as to its cause. The contrast in a bright-field TEM image, $C=(I_1-I_2)I_1$, is given by equation (2) (where $I_1>I_2$)

$$C=\frac{\exp[-S_p\rho_1(x,y)t_1(x,y)]-\exp[-S_p\rho_2(x,y)t_2(x,y)]}{\exp[-S_p\rho_1(x,y)t_1(x,y)]}, \tag{2}$$

where S_p is the effective mass thickness scattering cross-section ($cm^3\,nm^{-1}\,gm^{-1}$), $\rho(x,y)$ is the density, assumed to be variable only in the x,y plane, and $t(x,y)$ is the thickness. The value of S_p (0·0067) depends only on the accelerating voltage and the objective aperture size. The measured contrast from an in-focus image (see figure 4(*c*)) after steady state beam damage was $C=0{\cdot}24$. If one assumes a density of $1{\cdot}2\,g\,cm^{-3}$, a thickness difference of 34 nm would account for the observed contrast. If one assumes a constant section thickness of 80 nm, then a change in density of $\pm 0{\cdot}51\,g\,cm^{-3}$ would account for the observed contrast.

Large changes in chemical composition can occur for organic systems, especially those possessing ester and ether bonds, with exposure to high energy electrons [24]. In such polyesters and polyethers, substantial mass loss and crosslinking are observed at high electron dose. To determine if mass loss occurs in our sample, an intense beam was focused onto a small region wherein contrast rapidly developed. Upon expanding the

beam, the surrounding regions also developed contrast whose intensity was somewhat decreased relative to the small region indicating some enhanced mass loss (likely due to beam heating). Microdensitometry shows that the dark/white band image contrast is approximately the same in both regions. AFM experiments on irradiated sections were done to determine if locally $\Delta t(x, y)$ was preferentially affected by radiation damage. Height profile analysis indicated no significant change in the corrugation height (15–25 nm) with electron exposure, thereby eliminating large thickness changes as the sole source for the increase in contrast. Radiation damage effects on density and thickness cannot, at this stage, be separated, and thus, the large increase in contrast with electron dose observed for these cholesteric systems must arise from changes in the projected sample density, $\Delta(\rho(x, y)t(x, y))$. Due to the anisotropic nature of the cholesteric phase, these changes alter the projected density periodically, giving rise to the spatially varying contrast. Since previously reported BFTEM images of cholesteric morphology were probably obtained without taking precautions to minimize radiation damage, it is likely that the contrast mechanism in these previous studies is similar to the results presented here.

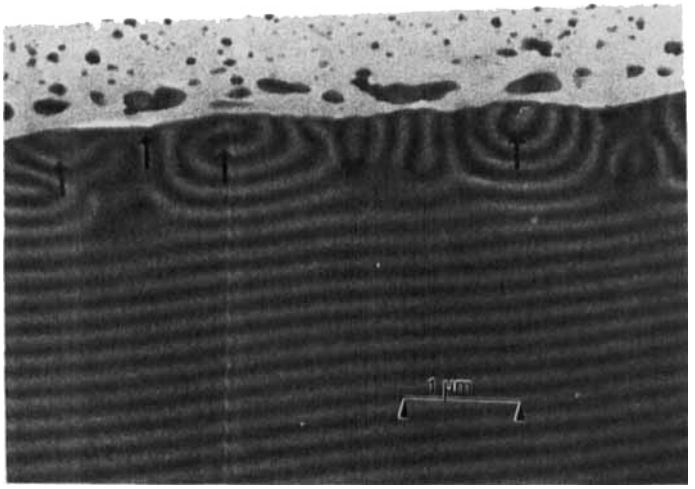

(*a*)

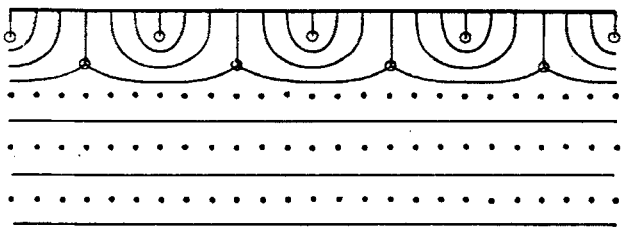

(*b*)

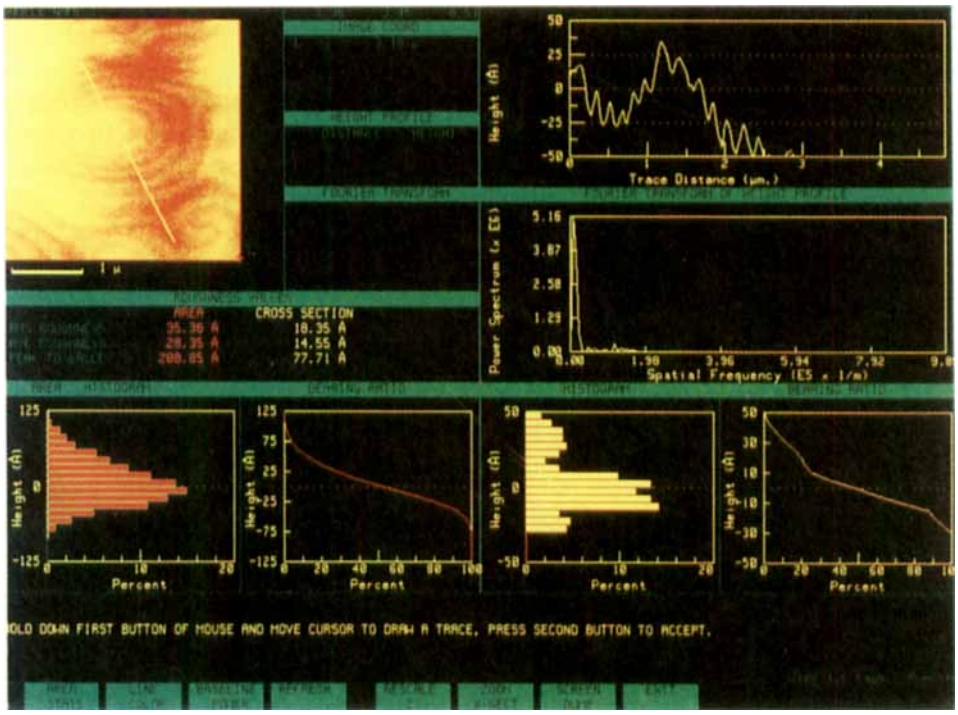

(*c*)

Figure 6. (*a*) TEM image of surface showing series of $+1/2$ and $-1/2$ disclinations and periodic surface topography (one-half the pitch). (*b*) Schematic of a vertical section through twisted planar texture. Note the surface is regarded as smooth [25]. (*c*) AFM image of surface of cast film. A complex topography is observed whose periodicity is one-half the pitch. The peak to valley height is an order of magnitude lower than that exhibited by the microtomed sections in figure 5.

Figure 7. LVHRSEM (0·8 keV) micrograph of bulk fracture surface from the sample investigated.

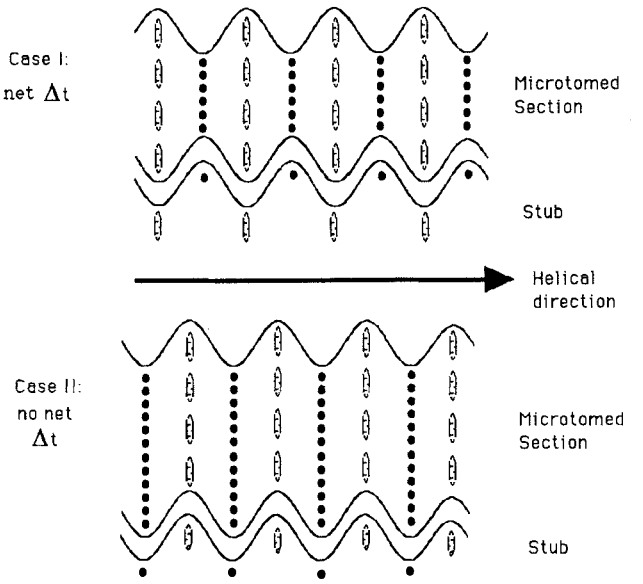

Figure 8. Two possible thickness variations in microtomed sections arising from preferential crack propagation in anisotropic cholesteric materials.

4. Conclusions

Due to the periodic anisotropy of the orientation of molecules, there is competition between forming a flat surface and propagating a crack across the fewest molecules during microtoming of cholesteric liquid crystalline glasses. The corrugated topography (LVHRSEM, AFM) and alternating bright and dark bands (TEM) are observed when the fracture path is parallel or oblique to the helical axis. The corrugated surface topography observed in LVHRSEM and AFM data from microtomed sections, microtomed stubs, and bulk fracture surfaces suggests the nature of the fracture is the same for all of the above described methods of sample preparation for these glassy materials.

Two different surface height corrugations were observed with AFM. Examination of fractured surfaces or microtomed samples (parallel to helix) indicate a peak to valley height of 20–25 nm with a spatial periodicity of $P/2$. Examination of the free surface of a glassy film indicates peak to valley heights of the order of 2–4 nm (also with a spatial periodicity of $P/2$), indicating a rotation of the helices near the surface. Although this height variation was below the resolution of LVHRSEM, TEM confirmed this reorientation and indicated a series of alternating $+1/2$ and $-1/2$ disclination lines at the surface of cast films.

Low dose TEM experiments indicate that little image contrast is present in minimally irradiated samples. Under typical viewing conditions, electron beam damage causes a rapid enhancement of the contrast. AFM experiments on irradiated samples showed no observable changes in the surface topography, so the increase in contrast must arise from a net change in the projected density, $\Delta(\rho(x, y)t(x, y)$, which is a function of both density and thickness.

The authors wish to thank Mary Jane O'Rourke for information on Grandjean free surfaces. ELT acknowledges support from NSF DMR 92-01845, AFOSR 90-0150, and AFOSR 91-0078 grants.

References

[1] GIRAUD-GUILLE, M.-M., 1988, *Calcif. Tissue Int.*, **42,** 16.
[2] GIRAUD-GUILLE, M.-M., 1987, *Molec. Crystals liq. Crystals*, **153,** 15.
[3] GIRAUD-GUILLE, M.-M., 1992, *J. molec. Biol.*, **224,** 861.
[4] VOIGT-MARTIN, I. G., DURST, H., and KLUG, H., 1989, *Macromolecules*, **22,** 595.
[5] VOIGT-MARTIN, I. G., and DURST, H., 1989, *Macromolecules*, **22,** 168.
[6] VOIGT-MARTIN, I. G., SIMON, P., GARBELLA, R. W., RINGSDORF, H., and TSCHIRNER, P., 1991, *Makromolek Chem. rap. Commun.*, **12,** 285.
[7] VOIGT-MARTIN, I. G., GARBELLA, R. W., and SCHUMACHER, M., 1992, *Macromolecules*, **25,** 961.
[8] THOMAS, E. L., and WOOD, B. A., 1985, *Faraday Discuss. chem. Soc.*, **79,** 229.
[9] HUDSON, S. D., VEZIE, D. L., and THOMAS, E. L., 1990, *Makromolek Chem. rap. Commun.*, **11,** 657.
[10] ADAMS, W. W., VEZIE, D. L., and THOMAS, E. L., 1992, *EMSA Proc.*, **50,** 266.
[11] SPONG, J. K., LACOMB, L. J., DOVEK, M. M., FROMMER, J. E., and FOSTER, J. S., 1989, *J. Phys.*, **50,** 2139.
[12] FOSTER, J. S., and FROMMER, J. E., 1988, *Nature, Lond.*, **333,** 542.
[13] VOSS, J., and VOSS, B., 1976, *Z. Naturf.*, **31,** 1661.
[14] BUNNING, T. J., KLEI, H. E., SAMULSKI, E. T., CRANE, R. L., and LINVILLE, R. J., 1991, *Liq. Crystals*, **10,** 445.
[15] COSTELLO, M. J., MEIBOOM, S., and SAMMON, M., 1984, *Phys. Rev.* A, **29,** 2957.
[16] BERREMAN, D. W., MEIBOOM, S., ZASADZINSKI, J. A., and SAMMON, M. J., 1986, *Phys. Rev. Lett.*, **57,** 1737.
[17] HARA, H., SATOH, T., TOYA, T., IIDA, S., ORII, S., and WATANABE, J., 1988, *Macromolecules*, **21,** 14.
[18] GIASSON, J., REVOL, J.-F., RITCEY, A. M., and GRAY, D. G., 1988, *Biopolym.*, **27,** 1999.
[19] GILLI, J. M., KAMAYE, M., and SIXOU, P., 1989, *J. Phys., France*, **50,** 2911.
[20] SIXOU, P., GILLI, J. M., TEN BOSCH, A., FRIED, F., MAISSA, P., VARICHON, L., and GODINHO, M. H., 1991, *Physica scripta*, **T35,** 47.
[21] BUNNING, T. J., 1992, Ph.D. Dissertation, University of Connecticut.
[22] DAVE, V., GLASSER, W. G., and WILKES, G., 1992, *Polym. Bull.*, **29,** 565.
[23] REIMER, L., 1965, *Laboratory Investigation: J. Path.*, **14,** 344.
[24] BAHR, G. F., JOHNSON, F. B., and ZEITLER, E., 1965, *Laboratory Investigation: J. Path.*, **14,** 377.
[25] SAUPE, A., 1973, *Molec. Crystals liq. Crystals*, **21,** 211.
[26] ZASADZINSKI, J. A. N. (personal communication).